Iraqi Journal of Natural Sciences and Nanotechnology IJNSN

# Studying the Effect of the Geomagnetic Storm (Solar Cycle 24) On the Radio Wave Propagation Through the Ionosphere

**Ali Hussein Nima[1] , Aqeel Gazi Mutar[2]**
[1] Research and Development Department Ministry of Higher Education and Scientific Research. Baghdad, Iraq,
[2] Department of Atmospheric Sciences, University of Mustansiriyah, College of Science, Baghdad, Iraq,
*Corresponding Author :* dr.alinima@rdd.edu.iq.

**Keywords:**

*Ionosphere; Geomagnetic Storm; Radio wave Propagation; Maximum Usable Frequency; Solar Cycle;*

**Abstract**

Identifying the ionospheric parameters is one of the important topics in the field of communication support services. In this paper, the Maximum Usable Frequency at 3000 km of the F2 layer (identified as MUF(3000)F2) for high-frequency radio wave propagation has been studied according to its correlation with the Geomagnetic Activity represented by a factor called the Disturbance Solar Time (Dst). Only fifteen disturbed and quiet events of geomagnetic activity associated with the availability of hourly variation of MUF(3000) F2 for three ionosonde station sites have been selected. The three available sites of ionosonde stations are Eglin AFB (30.5° N, 273.45° W), San Vito (40.6° N, 17.8° E), and Dourbes (50.1° N, 4.6° E), and the hourly variations of MUF (3000) F2 were calculated during 2012–2016. The values of the correlation coefficient (CC) were higher and a positive correlation for disturbed events than for quiet events. Geographically, the correlation between the MUF(3000)F2 and the disturbance solar time (Dst) increases with increasing latitude from Eagle AFB to Dourbes. For Eagle AFB and San Vito stations, the values of CC equal (0.473842, -0.21695) for disturbed activity, which relate to positive and negative correlation, respectively. In contrast, for quiet activity, the values of cc equal (-0.36477, 0.15829), respectively. For the high-latitude station (Dourbes), for both disturbed and quiet activity, the correlation between the average value of MUF(3000)F2 and average Dst has a negative correlation (CC=-0.2626, 0.2718). Increasing geomagnetic activity has no significant effect on the average MUF(3000)F2 values. The main shortcomings of this study are the unavailability of the entire dataset and the MUF(3000)F2 related to geomagnetic disturbances, which is represented by the Dst, thereby affecting a comprehensive analysis of the relationship between the above parameters.

## Introduction

The ionosphere is the layer of the atmosphere between 60 and 1000 km above Earth's surface. It consists of three different regions, called D, E, and F layers, which are separated into F1 & F2 layers

[1]. At any moment, different properties of the ionosphere can be measured and used to make predictions of radio activity and long-distance propagation. The critical frequency ($f_C$) and maximum usable frequency (MUF) present the state of ionization and the ability of communications. These frequencies increase after sunrise, enabling communications at higher and higher frequencies with the sun. The critical frequency, $f_{C,}$ is the highest frequency that can be reflected when a signal strikes the ionosphere normally [2].

The ionosphere is a region that can affect the propagation of radio waves due to variations in radio refractive index, which is related to the electron concentration [3]. The Maximum Usable Frequency (MUF) is the highest radio frequency that can be used for skywave communication between two terminals on Earth's surface. MUF is the product of F2-layer critical frequency (foF2) and Propagation factor M(3000)F2 [4].

Space weather alludes to conditions on the Sun, in the solar wind, and within Earth's magnetosphere, ionosphere, and thermosphere that can impact the reliability of space-borne and ground-based technological systems. The charged particles travel from the Sun more slowly, from a few hours to several days. Geomagnetic and ionospheric storms can cause interruption to Global Positioning System (GPS) navigation, malfunction of satellites, and HF-communication systems [5].

Influenced by the substantial energy influx from geomagnetic storms, ionospheric storms result in fluctuations in electron density, impacting societal functions and the space environment. This includes significant ionospheric correction errors for trans-ionospheric radio signals, disruption of High Frequency (HF) communication systems, and interference with Ultra High Frequency (UHF) satellite communications [6].

D.R. Lakshmi et al. [7] donate a storm-time model to HF communication users at low latitudes so that they can update their median predictions whenever active magnetic conditions are expected. S.E. Milan et al. [8] operated within the HF-band fourteen frequencies that were transmitted each hour for two 24-day pilot programs during the summer of 1988 and the winter of 1989. To determine signal recognition and signal strength, the received signals were analyzed and compared with the quiet-time comportment of the propagation. J. Lastovick [9] Depending on three districts according to the effects of the geomagnetic storm on the mid-latitude ionosphere: strong effect with positive and negative phases for the F2-region, weak and less known effect for the F1-E region, and strong positive effect for the lower ionosphere.

Elijah O. Oyeyemi et al [10]; A different implementation of neural networks (NNS) has been clarified, which led to developing a global model of the ionospheric propagation factor M(3000)F2 for different stations through the duration (1964-1986)

Mon-Lian Zhang et al. [11] describe the empirical orthogonal function expansion method for global modeling of M(3000)F2. The monthly median hourly values of M(3000)F2 for the period 1975-1985 have been used.

M.C. Walden [12], Chilton ionosonde critical frequency measurements have been compared with vertical-incidence HF-propagation predictions using the Voice of America Coverage Prediction Program System and the Advanced Stand-Alone Prediction System for solar cycle 23. D.V. Blagoveshchenskii [13], the main ionospheric effect during geomagnetic storms (sub-storms) in the character of decameter-wave propagation has been analyzed.

Jonas R. Souza et al. [14] calculate the MUF using the parameters foF2 and hmF2 and spherical geometry. The ionograms and a parameterized Regional Ionospheric Model (PARIM) have been used to obtain the above parameters. Leo F. McNamara and Donald C. Thompson [15] present the comparison between the COSMIC and ionosonde values of M(3000)F2, as well as the radio occultation and ionosonde observations, and the procedure.

N.M. Polekh et al. [16] studied the variations of parameters in the ionosphere and thermosphere for sub-auroral latitudes during March 17-19, 2015. D.V. Blagoveshchenskii [17]. Three near-polar radio

paths and one additional high-latitude path have been adopted during geomagnetic disturbances to investigate the response of HF radio wave propagation.
D.V. Blagoveshchenskii et al. [18] clarify the effect of the ionosphere on radio propagation during March 17-19, 2015, for paths located in the zone of North Siberia in Russia and have different lengths from 1000 to 5000 km. V.P. Uryadov et al. [19] illustrate the influence of the Powerful magnetic storm and X-ray bursts in 2015 on the Attributes of HF signals.
Ana G. Elias et al. [20] evaluating the influence of Earth's magnetic field on the M(3000)F2 factor and its consequences for hmF2 estimation," and "analyzing the systematic errors in hmF2 derived from M(3000)F2 due to geomagnetic field variations. Hongmei Bai et al. [21] developed a new extreme learning machine (ELM) model to forecast the ionospheric propagation factor M(3000)F2 at Darwin, Australia, using data from 1998–2014, excluding 2001 and 2009.
The Disturbance Storm Time (Dst) index is a physical quantity in units of nanoTesla (nT). The magnitude of the Dst index varied an extremely small negative integer that indicated a large geomagnetic storm. Thus, the large, sharpened variants of negative Dst indices could describe the detailed features of a Geomagnetic Storm. The Dst index was estimated from the measurements obtained at stations based on the International Real Time Magnetic Observatory Network (INTERMAGNET) [22]. Space weather and its effect on the ionosphere depend on solar radiation and the parameters of the solar wind (SW) and the interplanetary magnetic field (IMF) in both quiet and disturbed conditions [23]. Users of satellite navigation and satellite communications systems must assess and monitor ionospheric effects, which may degrade their performance. [24].
The efficient transfer of energy from solar wind outbursts from active regions of the Sun into the Earth's magnetosphere generates major disturbances referred to as geomagnetic storms. Such disturbances translate into perturbations of the charged particles of the ionosphere and can cause detrimental effects on radio wave signals and satellite communications [25]. Geomagnetic storms evolve in three phases: 1. The initial phase is an abrupt positive variation in the Dst index, called Sudden Storm Commencement (SSC). An (SSC) is produced by sudden compression in the magnetosphere caused by an increment of the dynamic pressure of the Solar wind. 2. The main phase where the Dst index takes the negative values during the injection of energized plasma in the equatorial ring current until it reaches a minimum Dst value; and 3. The recovery phase, where Dst values increase until they reach pre-sudden commencement values during the return of the geomagnetic field to normality [26].
The main goal of this study is to investigate the effect of the Geomagnetic Storm (Solar cycle 24) on the Maximum usable frequencies for communication through the Ionosphere.

The ionosphere is the layer of the atmosphere between 60 and 1000 km above Earth's surface. It consists of three different regions, called D, E, and F layers, which are separated into F1 & F2 layers [1]. At any moment, different properties of the ionosphere can be measured and used to make predictions of radio activity and long-distance propagation. The critical frequency ($f_C$) and maximum usable frequency (MUF) present the state of ionization and the ability of communications. These frequencies increase after sunrise, enabling communications at higher and higher frequencies with the sun. The critical frequency, $f_C$, is the highest frequency that can be reflected when a signal strikes the ionosphere normally [2].
The ionosphere is a region that can affect the propagation of radio waves due to variations in radio refractive index, which is related to the electron concentration [3]. The Maximum Usable Frequency (MUF) is the highest radio frequency that can be used for skywave communication between two terminals on Earth's surface. MUF is the product of F2-layer critical frequency (foF2) and propagation factor M(3000)F2 [4].
Space weather alludes to conditions on the Sun, in the solar wind, and within Earth's magnetosphere, ionosphere, and thermosphere that can impact the serviceability of space-borne and ground-based

technological systems. The charged particles travel from the Sun more slowly, from a few hours to several days. Geomagnetic and ionospheric storms can cause interruption to Global Positioning System (GPS) navigation, malfunction of satellites, and HF-communication systems [5]. Guided by the high energy inputs from geomagnetic storms, the ionospheric storms result in varying electron density and have effects on society and on the space environment, including high ionospheric correction error for trans-ionospheric radio signals, stifling of High Frequency (HF) communication systems, and upset of Ultra High Frequency (UHF) satellite communications [6].

D.R. Lakshmi et al. [7] donate a storm-time model to HF communication users at low latitudes so that they can update their median predictions whenever active magnetic conditions are expected. S.E. Milan et al. [8] operated within the HF band on fourteen frequencies that were transmitted each hour for two 24-day pilot programs during the summer of 1988 and the winter of 1989. To determine signal recognition and signal strength, the received signals were analyzed and compared with the quiet-time comportment of the propagation. J. Lastovick [9] Depending on three districts according to the effects of the geomagnetic storm on the mid-latitude ionosphere: a strong effect with positive and negative phases for the F2-region, a weak and less known effect for the F1-E region, and a strong positive effect for the lower ionosphere.

Elijah O. Oyeyemi et al. [10]; a different implementation of neural networks (NNs) has been clarified, which led to developing a global model of the ionospheric propagation factor M(3000)F2 for different stations through the duration (1964-1986).

Mon-Lian Zhang et al. [11] describe the empirical orthogonal function expansion method for global modeling of M(3000)F2. The monthly median hourly values of M(3000)F2 for the period 1975-1985 have been used.

M.C. Walden [12], Chilton ionosonde critical frequency measurements have been compared with vertical-incidence HF-propagation predictions using the Voice of America Coverage Prediction Program System and the Advanced Stand-Alone Prediction System for solar cycle 23. D.V. Blagoveshchenskii [13], the main ionospheric effect during geomagnetic storms (substorms) in the character of decameter-wave propagation has been analyzed.

Jonas R. Souza et al. [14] calculate the MUF using the parameters foF2 and hmF2 and spherical geometry. The ionograms and a parameterized Regional Ionospheric Model (PARIM) have been used to obtain the above parameters. Leo F. McNamara and Donald C. Thompson [15] present the comparison between the COSMIC and ionosonde values of M(3000)F2, as well as the radio occultation and ionosonde observations, and the procedure.

N.M. Polekh et al. [16] studied the variations of parameters in the ionosphere and thermosphere for sub-auroral latitudes during March 17-19, 2015. D.V. Blagoveshchenskii [17]. Three near-polar radio paths and one additional high-latitude path have been adopted during geomagnetic disturbances to investigate the response of HF radio wave propagation.

D.V. Blagoveshchenskii et al. [18] clarify the effect of the ionosphere on radio propagation during March 17-19, 2015, for paths located in the zone of North Siberia in Russia and have different lengths from 1000 to 5000 km. V.P. Uryadov et al. [19] illustrate the influence of the powerful magnetic storm and X-ray bursts in 2015 on the attributes of HF signals.

Ana G. Elias et al. [20] evaluating the influence of Earth's magnetic field on the M(3000)F2 factor and its consequences for hmF2 estimation and "analyzing the systematic errors in hmF2 derived from M(3000)F2 due to geomagnetic field variations." Hongmei Bai et al. [21] developed a new extreme learning machine (ELM) model to forecast the ionospheric propagation factor M(3000)F2 at Darwin, Australia, using data from 1998–2014, excluding 2001 and 2009.

The Disturbance Storm Time (Dst) index is a physical quantity in units of nanoTesla (nT). The magnitude of the Dst index varied an extremely small negative integer that indicated a large geomagnetic storm. Thus, the large, sharpened variants of negative Dst indices could describe the detailed features of a geomagnetic storm. The Dst index was estimated from the measurements

obtained at stations based on the International Real-Time Magnetic Observatory Network (INTERMAGNET) [22]. Space weather and its effect on the ionosphere depend on solar radiation and the parameters of the solar wind (SW) and the interplanetary magnetic field (IMF) in both quiet and disturbed conditions [23]. Users of satellite navigation and satellite communications systems must assess and monitor ionospheric effects, which may degrade their performance. [24].
The efficient transfer of energy from solar wind outbursts from active regions of the Sun into the Earth's magnetosphere generates major disturbances referred to as geomagnetic storms. Such disturbances translate into perturbations of the charged particles of the ionosphere and can cause detrimental effects on radio wave signals and satellite communications [25]. Geomagnetic storms evolve in three phases:1. The initial phase is an abrupt positive variation in the Dst index, called Sudden Storm Commencement (SSC). An SSC is produced by sudden compression in the magnetosphere caused by an increment of the dynamic pressure of the solar wind. 2. The main phase, where the Dst index takes the negative values during the injection of energized plasma in the equatorial ring current until it reaches a minimum Dst value; and 3. The recovery phase, where Dst values increase until they reach pre-sudden commencement values during the return of the geomagnetic field to normality [26].
This study's primary objective is to examine how the Geomagnetic Storm (Solar Cycle 24) affects the highest frequencies that can be used for ionosphere-based communication.

## Data and Methods of Analysis

The Global Ionospheric Radio Observatory (GIRO) Portal provided the MUF data. 30 million recordings of ionospheric measurements taken at 64 sites are made available to the public by Today (GIRO), 42 of which offer real-time streams, disseminating their measurement results a few minutes after they are finished [27]. The GIRO is available online at (http://www.giro.uml.edu/index.html). In cooperation with the (URSI) Ionosonde Network Advisory Group (INAG), the LGDC (Lowell GIRO Data Centre) promotes cooperative agreements with the ionosonde observations of the world to accept and process real-time data of HF radio monitoring the ionosphere and to promote a variety of investigations that benefit from the global scale, prompt, detailed, and accurate descriptions of the ionospheric variability. Most of the ionosonde stations are located on the continents and islands in order to cover the world (Figure 1).


Figure 1 GIRO Ionosonde Stations

The dataset utilized to examine the correlation between MUF(3000)F2 and geomagnetic storm events comprises daily hourly values of MUF(3000)F2, contingent upon data availability, from ionosonde stations worldwide, spanning the period from December 2008 to December 2019 (solar cycle 24); this also covered all quiet and erratic magnetic activity phases. The ionosonde stations supporting the above-mentioned time have been analyzed.

Table 1 Ionosonde stations supported with periods of solar cycle (24)

| index | Station Name | Station Code | Latitude (deg) | Longitude (deg) | Period of Data Used |
|---|---|---|---|---|---|
| 1 | Hermanus | HE13N | -34.42 | 19.22 | 2002-2023 |
| 2 | Grahamstown | GR13L | -33.3 | 26.5 | 1996-2023 |
| 3 | Paulista | CAJ2M | -22.7 | 315 | 2000-2024 |
| 4 | Learmonth | LM42B | -21.8 | 114 | 1999-2023 |
| 5 | Jicamarca | JI91j | -12 | 283.2 | 1993-2022 |
| 6 | Ascension island | AS00Q | -7.94 | 345.6 | 1997-2024 |
| 7 | Fortalezao | FZA0M | -3.9 | 321.6 | 2009-2024 |
| 8 | Ramey | PRJ18 | 18.5 | 292.9 | 1999-2022 |
| 9 | Austin | AU930 | 30.4 | 202.3 | 1999-2024 |
| 10 | Eaglin AFb | EG931 | 30.5 | 273.15 | 2009-2024 |
| 11 | Jeju | Jj433 | 33.43 | 126.3 | 20092024 |
| 12 | PT Arguello | PA836 | 34.8 | 239.6 | 2000-2024 |
| 13 | Nicosia | NI63 | 35.03 | 33.16 | 2008-2024 |
| 14 | Arenosillo | EA036 | 37.1 | 353.5 | 2004-2024 |
| 15 | I-Cheon | IC437 | 37.14 | 127.54 | 2010-2024 |
| 16 | Athens | AT138 | 38 | 23.5 | 2003-2024 |
| 17 | Boulder | BC840 | 40 | 254 | 1999-2024 |
| 18 | San Vito | VT139 | 40.6 | 17.8 | 2004-2024 |
| 19 | Requetes | EB040 | 40.8 | 0.3 | 2004-2024 |

| | | | | | |
|---|---|---|---|---|---|
| 20 | Rome | RM041 | 41.9 | 12.5 | 1997-2023 |
| 21 | Millstone Hill | MHj4 | 42.6 | 288.5 | 2000-2024 |
| 22 | Druhonica | PQ052 | 50 | 14.6 | 2004-2024 |
| 23 | Dourbes | DB049 | 50.1 | 4.6 | 2011-2024 |
| 24 | Chilton | RL052 | 51.5 | 359.4 | 1996-2024 |
| 25 | Fairford | FF051 | 51.7 | 359.4 | 1996-2024 |
| 26 | Juliusruh | JR055 | 54.6 | 13.4 | 2007-2024 |
| 27 | Gakona | GA762 | 62.38 | 215 | 1998-2024 |
| 28 | Tromso | TR169 | 69.9 | 19.2 | 1999-2024 |

There is no single description of the strength of the GSs concerning the (Dst) index, as the thresholds change across different authors: moderate ($50 \leq |Dst| \leq 100$ nT), intense ($100 \leq |Dst| \leq 250$ nT), and super storm ($|Dst| \geq 250$ nT) [28]. There are two primary categories of geomagnetic variations: geomagnetic disturbance, which is mostly caused by fast solar winds, and quiet variation, which is primarily caused by solar electromagnetic radiation and has a regular look [29].

A number of techniques have been put out to differentiate between peaceful and disturbed activities. When the index Dst is more than -30 nT, a day is considered geomagnetically peaceful; otherwise, it is considered disturbed [28]. The World Data Center for Geomagnetism, Kyoto Online Catalogue (http://wdc.kugi.kyoto-u.ac.jp/index.html) has the data of (Dst). We employed both quiet and disturbed geomagnetic storm occurrences from 2008 to 2019, with the disturbed days from the 2011–2018 geomagnetic event corresponding to the same month and year.

Table 2 The disturbed and adopted quiet geomagnetic storm events during the period 2008 to 2019

| index | Date | $Dst_{min}$ | $h_{min}$ | Date | $Dst_{max}$ | $h_{max}$ |
|---|---|---|---|---|---|---|
| 1 | 6/8/2011 | -115 | 4 | | | |
| 2 | 26/9/2011 | -118 | 24 | | | |
| 3 | 25/10/2011 | -147 | 2 | | | |
| 4 | 9/3/2012 | -145 | 9 | | | |
| 5 | 24/4/2012 | -120 | 5 | 30/4/2012 | -7 | 6 |
| 6 | 15/7/2012 | -139 | 17 | | | |
| 7 | 1/10/2012 | -122 | 5 | 4/10/2012 | -9 | 16 |
| 8 | 9/10/2012 | -109 | 9 | 20/10/2012 | 0 | 7 |
| 9 | 14/11/2012 | -108 | 8 | 9/11/2012 | 10 | 16 |
| 10 | 17/3/2013 | -132 | 21 | 8/3/2013 | 8 | 7 |
| 11 | 1/6/2013 | -124 | 9 | 16/6/2013 | 2 | 4 |
| 12 | 29/6/2013 | -102 | 7 | | | |
| 13 | 19/2/2014 | -119 | 9 | 13/2/2014 | 8 | 7 |
| 14 | 7/1/2015 | -107 | 12 | 20/1/2015 | 29 | 24 |
| 15 | 17/3/2015 | -234 | 23 | 30/3/2015 | -19 | 9 |
| 16 | 23/6/2015 | -198 | 5 | | | |
| 17 | 27/8/2015 | -103 | 21 | 14/8/2015 | -5 | 23 |
| 18 | 9/9/2015 | -105 | 13 | 27/9/2015 | 1 | 8 |
| 19 | 7/10/2015 | -130 | 23 | 26/10/2015 | 1 | 9 |
| 20 | 20/12/2015 | -166 | 23 | 30/12/2015 | 1 | 13 |
| 21 | 1/1/2016 | -110 | 1 | | | |

| | | | | | | |
|---|---|---|---|---|---|---|
| 22 | 20/1/2016 | -101 | 17 | 29/1/2016 | -6 | 14 |
| 23 | 13/10/2016 | -110 | 13 | 20/10/2016 | 1 | 11 |
| 24 | 28/5/2017 | -125 | 8 | | | |
| 25 | 8/9/2017 | -122<br>-109 | 2<br>18 | | | |
| 26 | 26/8/2018 | -175 | 7 | | | |

Hourly values of MUF(3000) F2 must be available for both the ionosonde station sites and through disturbances and quiet geomagnetic activity, as the primary objective is to investigate the relationship between the MUF(3000) F2 and the Dst for disturbed (Dst ≤ -100) and quiet (Dst > -30) geomagnetic events during the solar cycle (24) (24). However, because the data for the majority of the ionosonde sites were insufficient, not all events were adopted.
Under this criterion, only (15) disturbed and quiet events of geomagnetic activity associated with the availability of hourly variation of MUF(3000)F2 for three ionosonde station sites have been selected. Table (3) shows the ionosonde stations adopted in this study. The three available sites of ionosonde stations are Eglin AFB (30.5° N, 273.45° W), San Vito (40.6° N, 17.8° E), and Dourbes (50.1° N, 4.6° E), and the hourly variations of MUF(3000)F2 were calculated during 2012 to 2016.

Table 3 The only available three ionosonde stations have been adopted

| Index | Station Name | Station Code | Latitude (deg) | Longitude (deg) |
|---|---|---|---|---|
| 1 | Eaglin AFb | EG931 | 30.5 | 273.15 |
| 2 | San Vito | VT139 | 40.6 | 17.8 |
| 3 | Dourbes | DB049 | 50.1 | 4.6 |

For Comparison purposes, ionosonde measurements of MUF(3000)F2, the coefficient of variation was used to compare the variability of MUF during both disturbed and quiet geomagnetic activity through the solar cycle (24). The coefficient of variation, CV% (Variability), measures the variability in the values in the MUF(3000) F2 relative to the magnitude of its mean.
The coefficient of variation CV% is given by [30]:

$$VR = \frac{\sigma}{\mu} * 100\% \qquad (2)$$

Where $\sigma$ is the standard deviation, $\mu$ is the mean.

## Results and Discussion

From 2008 to 2019, a study was conducted at the aforementioned stations to examine the monthly and annual fluctuations of MUF(3000)F2 and its relationship to the solar disturbance time (Dst) throughout solar cycle 24. Only data from 2012 to 2016 were accessible due to technological issues, as the accompanying table illustrates.

Table 4 The Coefficient of Variation (VR %) for Disturbed and Quiet Geomagnetic Events during Solar Cycle 24 for Eagle AFB Station

| Event | Date | Average MUF | Average Dst | VR% | Date | Average MUF | Average Dst | VR% |
|---|---|---|---|---|---|---|---|---|
| 1 | 24/4/2012 | 24.73 | -75.458 | 7 | 30/4/2012 | 21.971 | -11.166 | 6.37 |
| 2 | 1/10/2012 | 19.668 | -74.958 | 17 | 4/10/2012 | 21.876 | -13.208 | 16.42 |
| 3 | 9/10/2012 | 18.1 | -73 | 3 | 20/10/2012 | 22.516 | -4 | 21.9 |
| 4 | 14/11/2012 | 23.932 | -67.625 | 1 | 9/11/2012 | 21.411 | 3.5416 | 7.7 |
| 5 | 17/3/2013 | 20.38 | -64.041 | 10 | 8/3/2013 | 21.637 | 3.375 | 11.1 |
| 6 | 1/6/2013 | 19.141 | -70.458 | 7 | 16/6/2013 | 20.982 | -0.7083 | 2.1 |
| 7 | 19/2/2014 | 22.488 | -66 | 34 | 13/2/2014 | 22.808 | 3.7083 | 17.23 |
| 8 | 7/1/2015 | 19.311 | -49.833 | 23 | 20/1/2015 | 22.12 | -3.666 | 5.43 |
| 9 | 17/3/2015 | 22.851 | -83.514 | 0.7 | 30/3/2015 | 23.909 | -25.208 | 29.2 |
| 10 | 27/8/2015 | 12.75 | -78.666 | 5 | 14/8/2015 | 16.839 | -11.625 | 4.7 |
| 11 | 9/9/2015 | 15.587 | -80.458 | 10 | 27/9/2015 | 20.121 | -4.875 | 20.8 |
| 12 | 7/10/2015 | 17.784 | -75.125 | 9 | 26/10/2015 | 21.11 | -8.1666 | 20.77 |
| 13 | 20/12/2015 | 22.556 | -73.083 | 9 | 30/12/2015 | 18.063 | -6.75 | 0.626 |
| 14 | 20/1/2016 | 19.284 | -54.083 | 3 | 29/1/2016 | 17.858 | -11.083 | 9.8 |
| 15 | 13/10/2016 | 20.3128 | -52.625 | 25.4 | 20/10/2016 | 17.895 | -5.2916 | 12.1 |

Table 5 The Coefficient of Variation (VR %) for Disturbed and Quiet Geomagnetic Events during Solar cycle 24 for Dourbes Station

| Event | Date | Average MUF | Average Dst | VR% | Date | Average MUF | Average Dst | VR% |
|---|---|---|---|---|---|---|---|---|
| 1 | 24/4/2012 | 13.021 | -75.458 | 3 | 30/4/2012 | 19.323 | -11.166 | 6.4 |
| 2 | 1/10/2012 | 13.403 | -74.958 | 8 | 4/10/2012 | 19.651 | -13.208 | 0.46 |
| 3 | 9/10/2012 | 15.543 | -73 | 0.3 | 20/10/2012 | 20.525 | -4 | 1.82 |
| 4 | 14/11/2012 | 10.316 | -67.625 | 4 | 9/11/2012 | 17.009 | 3.5416 | 3.28 |
| 5 | 17/3/2013 | 8.773 | -64.041 | 1.8 | 8/3/2013 | 20.32 | 3.375 | 0.59 |
| 6 | 1/6/2013 | 15.247 | -70.458 | 4.5 | 16/6/2013 | 21.097 | -0.7083 | 6.26 |
| 7 | 19/2/2014 | 18.337 | -66 | 6.6 | 13/2/2014 | 20.116 | 3.7083 | 0.94 |
| 8 | 7/1/2015 | 19.115 | -49.833 | 2.941 | 20/1/2015 | 19.663 | -3.666 | 3.7 |
| 9 | 17/3/2015 | 14.321 | -83.514 | 6.06 | 30/3/2015 | 18.904 | -25.208 | 3.36 |
| 10 | 27/8/2015 | 13.559 | -78.666 | 2.34 | 14/8/2015 | 16.533 | -11.625 | 6.3 |
| 11 | 9/9/2015 | 11.68 | -80.458 | 2.3 | 27/9/2015 | 18.793 | -4.875 | 1.54 |
| 12 | 7/10/2015 | 10.155 | -75.125 | 6.05 | 26/10/2015 | 19.418 | -8.1666 | 1.85 |
| 13 | 20/12/2015 | 13.504 | -73.083 | 3.35 | 30/12/2015 | 14.791 | -6.75 | 4.9 |
| 14 | 20/1/2016 | 16.465 | -54.083 | 3.74 | 29/1/2016 | 15.89 | -11.083 | 6.8 |
| 15 | 13/10/2016 | 17.916 | -52.625 | 1.22 | 20/10/2016 | 15.478 | -5.2916 | 0.913 |

Table 6 The Coefficient of Variation (VR %) for Disturbed and Quiet Geomagnetic Events during Solar Cycle 24 for San Vito Station

| Event | Date | Average MUF | Average Dst | VR% | Date | Average MUF | Average Dst | VR% |
|---|---|---|---|---|---|---|---|---|
| 1 | 24/4/2012 | 16.102 | -75.458 | 0.96 | 30/4/2012 | 21.38 | -11.166 | 2.5 |
| 2 | 1/10/2012 | 16.973 | -74.958 | 8.8 | 4/10/2012 | 20.57 | -13.208 | 2.226 |

| | | | | | | | | |
|---|---|---|---|---|---|---|---|---|
| 3 | 9/10/2012 | 22.146 | -73 | 3.21 | 20/10/2012 | 21.2 | -4 | 0.63 |
| 4 | 14/11/2012 | 12.843 | -67.625 | 0.33 | 9/11/2012 | 18.36 | 3.5416 | 9.4 |
| 5 | 17/3/2013 | 22.369 | -64.041 | 0.44 | 8/3/2013 | 21.29 | 3.375 | 1.79 |
| 6 | 1/6/2013 | 17.196 | -70.458 | 9.7 | 16/6/2013 | 22.64 | -0.7083 | 1.59 |
| 7 | 19/2/2014 | 20.965 | -66 | 10.65 | 13/2/2014 | 21.18 | 3.7083 | 0.33 |
| 8 | 7/1/2015 | 21.1 | -49.833 | 1.87 | 20/1/2015 | 21.06 | -3.666 | 1.51 |
| 9 | 17/3/2015 | 21.423 | -83.514 | 7.5 | 30/3/2015 | 22.22 | -25.208 | 0.69 |
| 10 | 27/8/2015 | 18.439 | -78.666 | 2.8 | 14/8/2015 | 17.99 | -11.625 | 2.5 |
| 11 | 9/9/2015 | 13.617 | -80.458 | 1.5 | 27/9/2015 | 19.85 | -4.875 | 0.67 |
| 12 | 7/10/2015 | 12.428 | -75.125 | 16.5 | 26/10/2015 | 20.27 | -8.1666 | 1.22 |
| 13 | 20/12/2015 | 18.806 | -73.083 | 3.12 | 30/12/2015 | 15.81 | -6.75 | 7.02 |
| 14 | 20/1/2016 | 19.747 | -54.083 | 4.08 | 29/1/2016 | 16.69 | -11.083 | 5.7 |
| 15 | 13/10/2016 | 20.466 | -52.625 | 3.45 | 20/10/2016 | 17.81 | -5.2916 | 1.46 |

## Average MUF versus Average Dst

To have a sense of the relationship between the MUF (3000) F2 and the (Dst) from 2012 to 2016. First, consider how the average MUF (3000) F2 value responds to the (Dst) for (15) events. The statistical average for MUF (3000) F2 and (Dst) for (15) observed events is displayed in Figures (2–7). The values of the correlation coefficients between MUF (3000) F2 and the disturbance solar time (Dst) are displayed in Table (7).

Table 7 The values of the coefficients of correlation between MUF (3000) F2 and the disturbance solar time (Dst)

| Index | Station | Disturbed | Quite |
|---|---|---|---|
| 1 | Eaglin AFb | 0.1277 | 0.0011507 |
| 2 | San Vito | 0.3749 | 0.00569 |
| 3 | Dourbes | 0.5298 | 0.1943 |

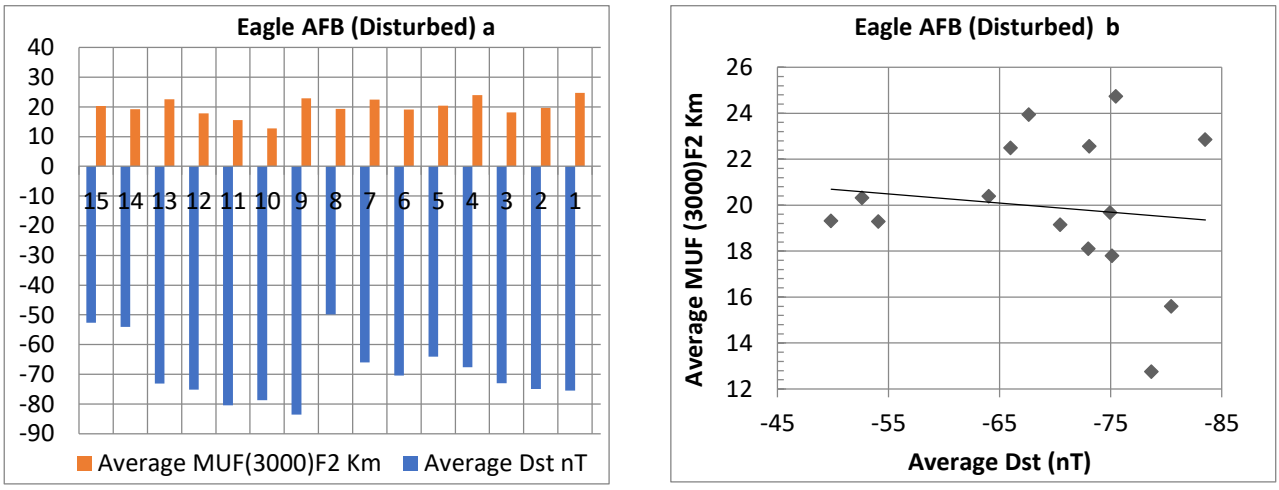


Figure 2 The statistical average value of MUF (3000) F2 to the Dst for Eagle AFB during disturbed (15) events. (a) Chart bar for both MUF (3000) F2 and Dst. (b) The correlation between the MUF (3000) F2 and Dst (CC=0.1277)

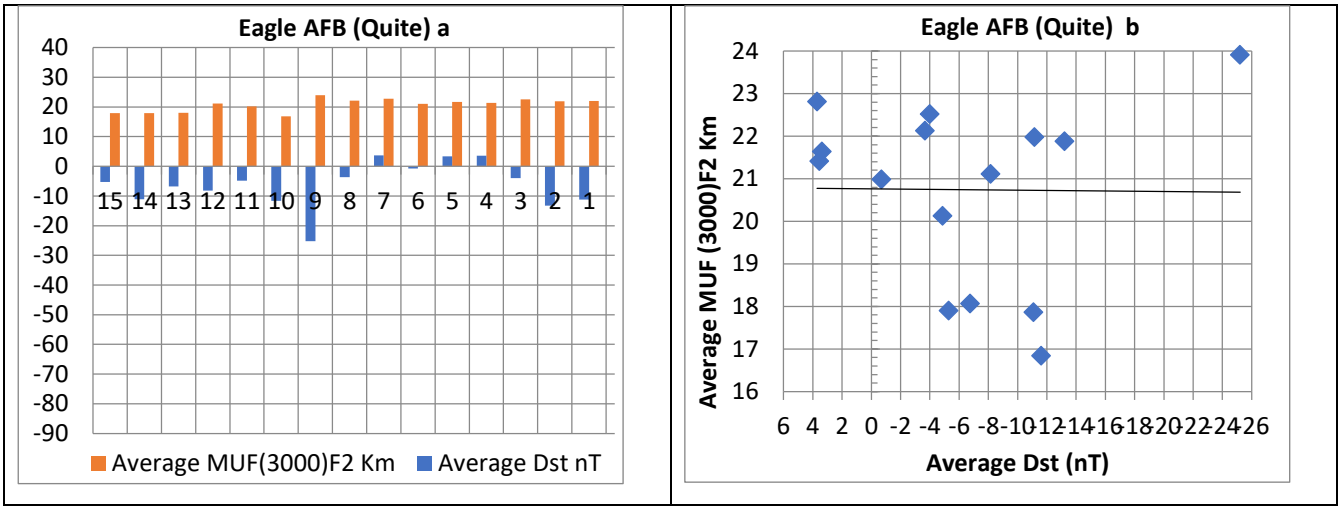


Figure 3 The statistical average value of MUF (3000) F2 to the Dst for Eagle AFB during Quiet (15) events. (a) Chart bar for both MUF (3000) F2 and Dst. (b) The correlation between the MUF (3000) F2 and Dst (CC=0.0115)

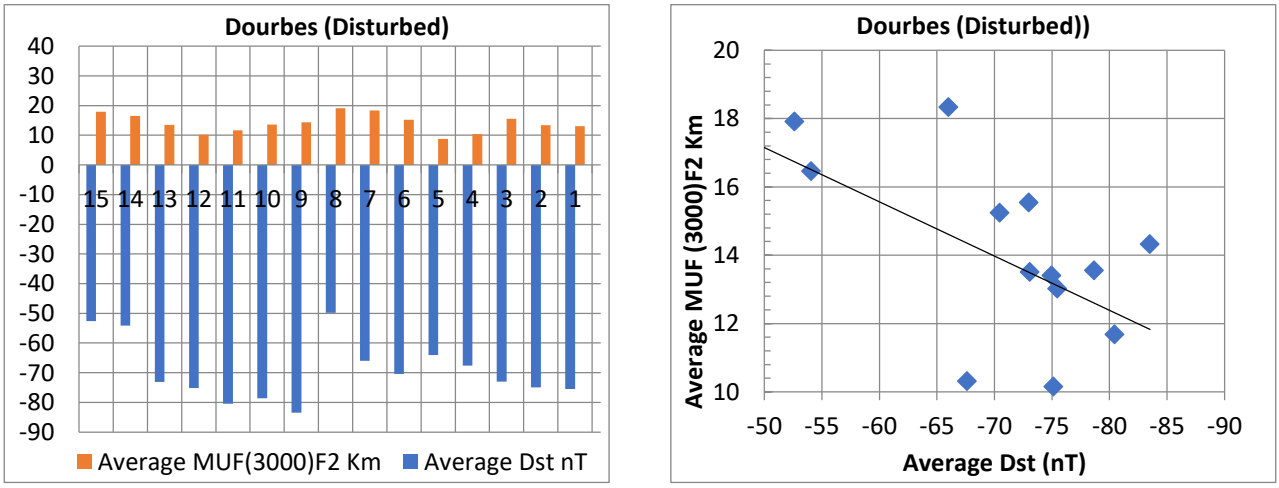


Figure 4 The statistical average value of MUF (3000) F2 to the Dst for Dourbes during Disturbed (15) events. (a) Chart bar for both MUF (3000) F2 and Dst. (b) The correlation between the MUF (3000) F2 and Dst (CC=0.5298)

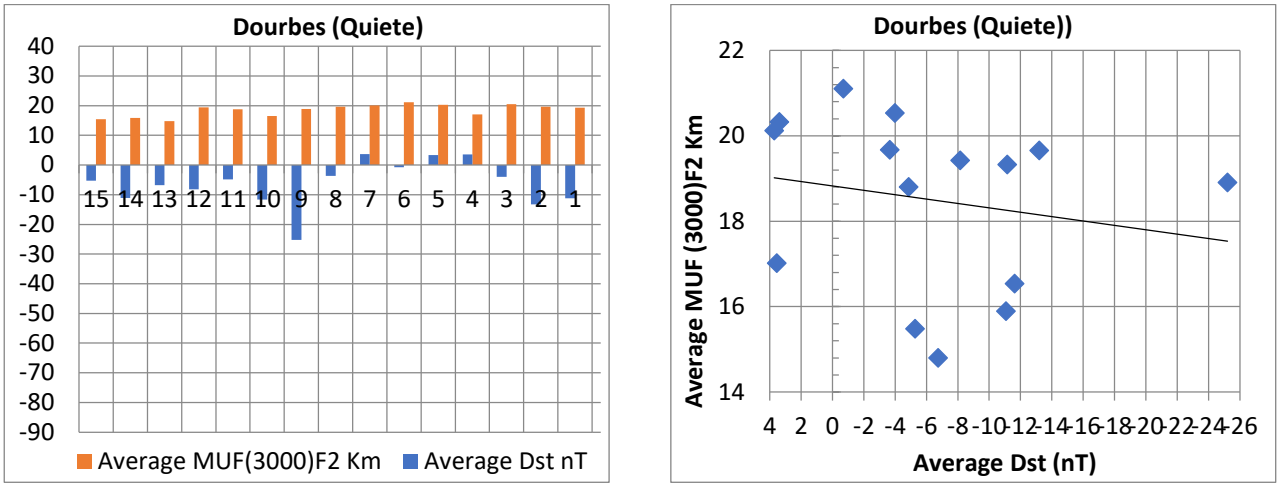


Figure 5 The statistical average value of MUF (3000) F2 to the Dst for Dourbes during Quiet (15) events. (a) Chart bar for both MUF (3000) F2 and Dst. (b) The correlation between the MUF (3000) F2 and Dst (CC=0.19436)

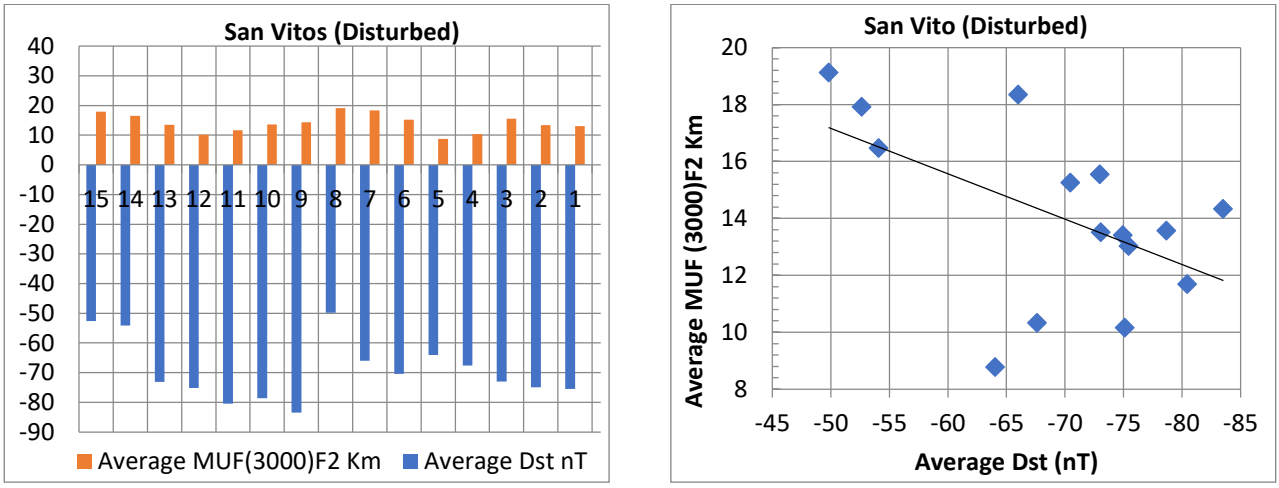


Figure 6 The statistical average value of MUF (3000) F2 to the Dst for San Vito during Disturbed (15) events. (a) Chart bar for both MUF (3000) F2 and Dst. (b) The correlation between the MUF (3000) F2 and Dst (CC=0.3749)

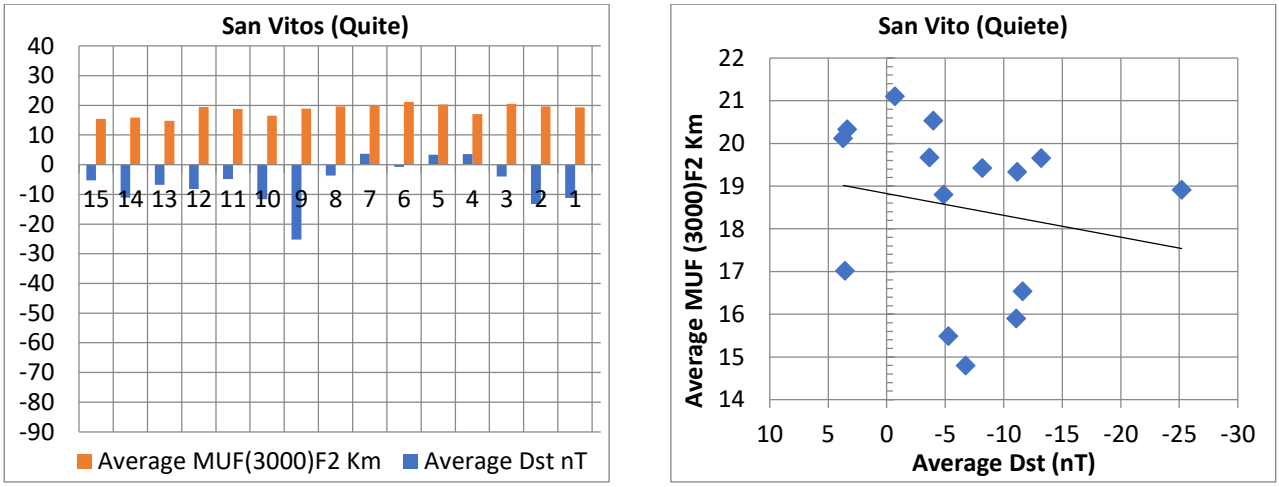


Figure 7 The statistical average value of MUF (3000) F2 to the Dst for San Vito during Quiet (15) events. (a) Chart bar for both MUF (3000) F2 and Dst. (b) The correlation between the MUF (3000) F2 and Dst (CC=0.00569)

From the statistical concept, the coefficient of correlation (CC) extends from -1 (negative correlation) to +1 (positive correlation). It is clear from figures (2, 4, and 6) for three sites (Eaglin AFB, Dourbes, and San Vito) for disturbed geomagnetic activity that the coefficients of correlation (CC) are equal to 0.1277, 0.5298, and 0.3749, respectively. While the figures (3, 5, and 7) represent the quiet geomagnetic activity with CC equal to (0.0115, 0.19436, 0.00569), there are no significant effects of increasing the geomagnetic activity on the values of the average of MUF(3000)F2. As well as the values of the CC, they were higher and had a positive correlation for disturbed events than quiet events. Geographically, the correlation between the MUF(3000)F2 and the disturbance solar time (Dst) increases with increasing latitude from Eagle AFB to Dourbes.

## VR% MUF versus Average Dst

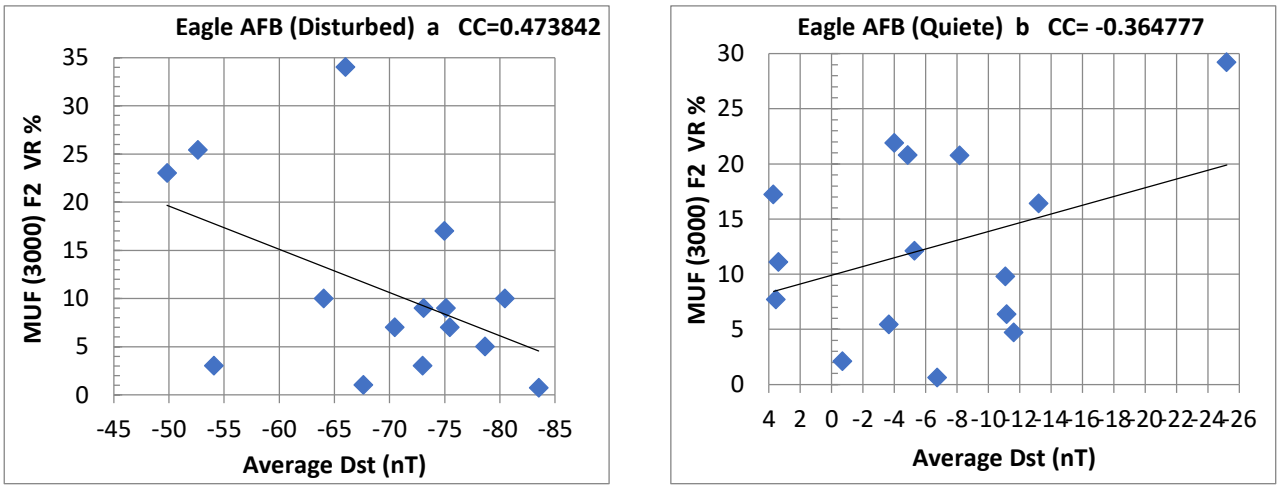


Figure 8 The average value of MUF (3000) F2 VR% against Dst for Eagle AFB during (a) Disturbed, (b) Quiet

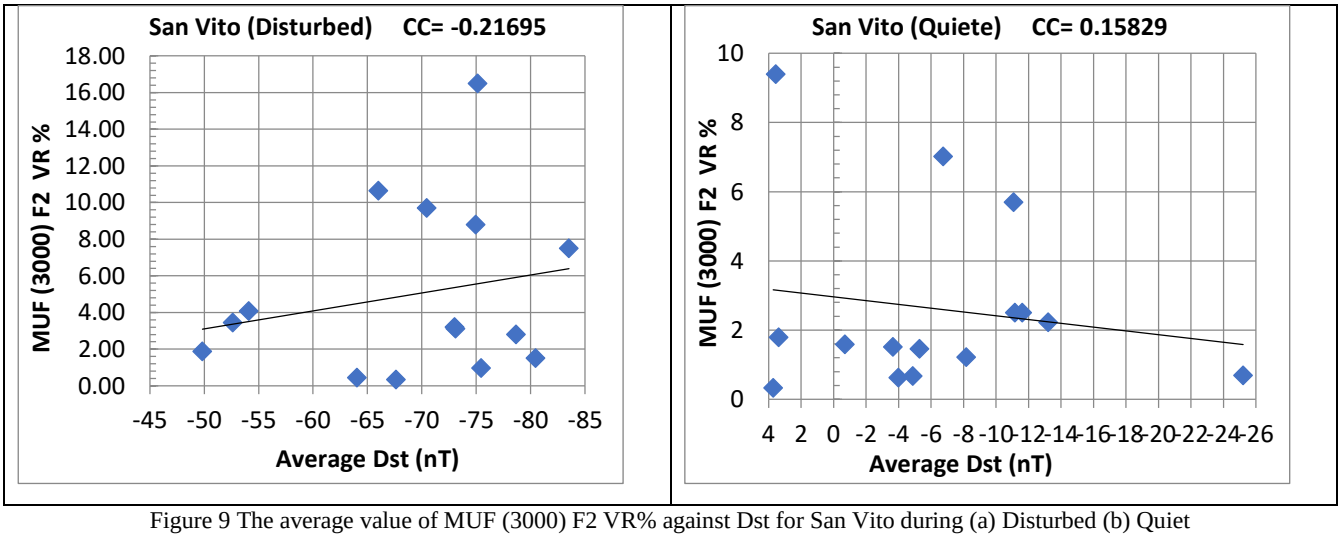


Figure 9 The average value of MUF (3000) F2 VR% against Dst for San Vito during (a) Disturbed (b) Quiet

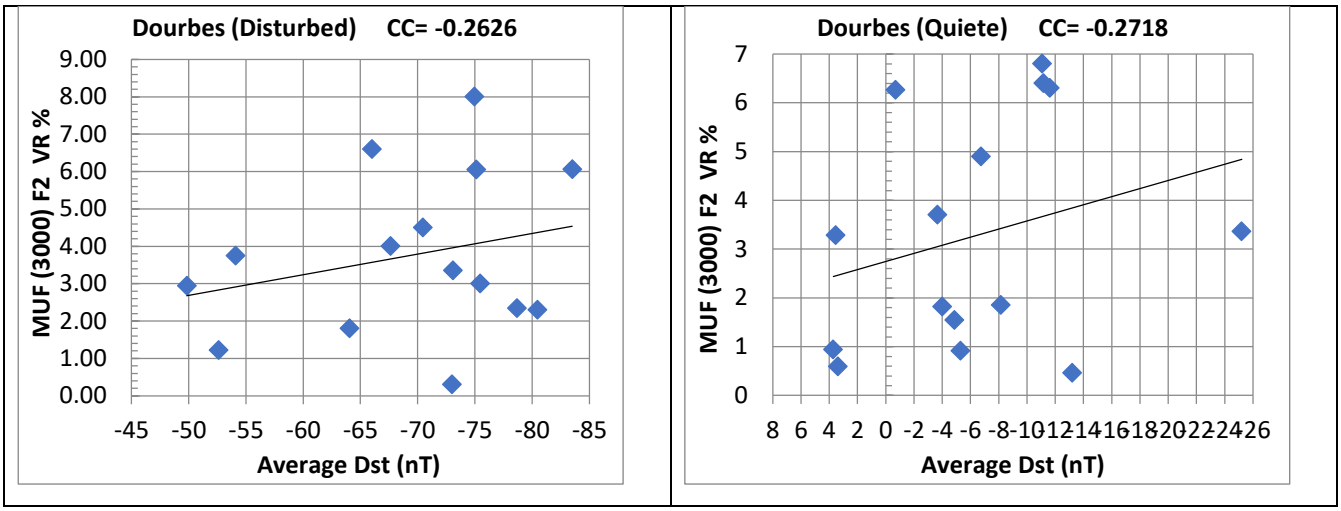


Figure 10 The average value of MUF (3000) F2 VR% against Dst for Dourbes during (a) Disturbed (b) Quiet

Figures (8-10) represent the variability ratio of the maximum usable frequency MUF(3000)F2 versus the average (Dst). For Eagle AFB and San Vito stations, the values of CC equal (0.473842, -0.21695) for disturbed activity, which relate to positive and negative correlation, respectively. In contrast, for quiet activity, the values of CC are equal (-0.36477, 0.15829) respectively. For the high latitude station (Dourbes), both disturbed and quiet activity, the correlation between the average value of MUF(3000)F2 and average (Dst) has a negative correlation (CC=-0.2626, 0.2718).

## CONCLUSION

In this study, only (15) disturbed and quiet events of geomagnetic activity associated with the availability of hourly variation of MUF(3000) F2 for three ionosonde station sites have been adopted. The three available sites of ionosonde stations are Eglin AFB (30.5° N, 273.45° W), San Vito (40.6° N, 17.8° E), and Dourbes (50.1° N, 4.6° E), and the hourly variations of MUF(3000)F2 were calculated from 2012 to 2016. After that, it is clear that no significant effects of increasing the geomagnetic activity on the values of the average of MUF(3000)F2. As well as the values of the correlation coefficient (CC) were higher and had a positive correlation for disturbed events than for quiet events. Geographically, the correlation between the MUF(3000)F2 and the disturbance solar time (Dst) increases with increasing latitude from Eagle AFB to Dourbes. For Eagle AFB and San Vito stations, the values of cc equal (0.473842, -0.21695) for disturbed activity, which relate to

positive and negative correlation, respectively. In contrast, for quiet activity, the values of CC are equal (-0.36477, 0.15829) respectively. For the high latitude station (Dourbes), both disturbed and quiet activity, the correlation between the average value of MUF(3000)F2 and average Dst has a negative correlation (CC=-0.2626 and 0.2718).

References

[1] Jian Wang, et al., A regional model for the prediction of M(3000) F2 over East Asia. Advances in Space Research, 2020; https://doi.org/10.1016/j.asr.2020.01.026.
[2] Karl F. Warnick, Joseph J. Carr, and George W. Hippisley, Practical Antenna Handbook 6th Edition, The McGraw-Hill Companies. 2025. ISBN: 9781260132250.
[3] Ankita, M., Tulasi Ram, S., Ajith, K.K., & Sripathi, S. Deep electron density depletion near sunset terminator on St. Patrick's Day storm and its impacts on Skywave propagation. Space Weather, (2023), 21, e2022SW003369. https://doi.org/10.1029/2022SW003369
[4] Zhang, Z., Yu, Q., Wang, J., Zhang, X., Zhu, Z., Zhao, L., & Yang, C. . Maximum usable frequency forecast model based on real-time oblique sounding data. Space Weather, (2025), 23, e2025SW004346.https://doi.org/10.1029/2025SW004346
[5] M. Pietrella and M. Pezzopane, Maximum usable frequency and skip distance maps over Italy, 2020, Advances in Space Research. https://doi.org/10.1016/j.asr.2020.03.040.
[6] Liu, Q., Hernández-Pajares, M., Lyu, H., Nishioka, M., Yang, H., Monte Moreno, E., et al. Ionospheric storm scale index based on high time resolution UPC-IonSAT global ionospheric maps (IsUG). Space Weather, (2021) 19, e2021SW002853. https:// doi.org/10.1029/2021SW002853
[7] D.R. LAKSHMI et al., A Prediction Model for Equatorial Low Latitude HF Communication Parameters during Magnetic Disturbances. Indian Journal of Radio & Space Physics, vol. 2, 1983, pp. 118-123.
[8] S. E. Milan et al., Observations of the four high latitude reduction in the available HF band on paths during periods of geomagnetic disturbance. Journal of Atmospheric and Solar-Terrestrial Physics 60 (1998) 617-629.
[9] J. Lastovicka, Monitoring and forecasting of ionospheric space weather effects of geomagnetic storms, Journal of Atmospheric and Solar-Terrestrial Physics 64 (2002) 697–705.
[10] Elijah O. Oyeyemi et al., Neural network-based prediction techniques for global modeling of M (3000)F2 ionospheric parameter, Advances in Space Research 39 (2007) 643–650.
[11] Man-Lian Zhang et al., Evaluation of global modeling of M(3000)F2 and hmF2 based on alternative empirical orthogonal function expansions, Advances in Space Research 46 (2010) 1024–1031.
[12] M. C. Walden, ANALYSIS OF CHILTON IONOSONDE CRITICAL FREQUENCY MEASUREMENTS DURING SOLAR CYCLE 23 IN THE CONTEXT OF MIDLATITUDE HF NVIS FREQUENCY PREDICTIONS, 12th IET International Conference on Ionospheric Radio Systems and Techniques (IRST 2012), York, UK, 15-17 May 2012. https://doi:10.1049/cp.2012.0373.
[13] D. V. Blagoveshchenskii, Effect of Magnetic Storms (Substorms) on HF Propagation: A Review, Geomagnetism and Aeronomy, 2013, Vol. 53, No. 4, pp. 409–423.
[14] Jonas R. Souza et al., "A Simple Method to Calculate the Maximum Usable Frequency," SEG Global Meeting Abstracts: (2013), 1874-1878. https://doi.org/10.1190/sbgf2013-386

[15] Leo F. McNamara and Donald C. Thompson, Validation of COSMIC values of foF2 and M(3000)F2 using ground-based ionosondes. Advances in Space Research 55 (2015) 163–169. http://dx.doi.org/10.1016/j.asr.2014.07.015.
[16] N. M. Polekh et al., Ionospheric Effects of Magnetospheric and Thermospheric Disturbances on March 17–19, 2015, Geomagnetism and Aeronomy, 2016, Vol. 56, No. 5, pp. 557–571.
[17] D. V. Blagoveshchenskii, Anomalous Phenomena on HF Radio Paths during Geomagnetic Disturbances, Geomagnetism and Aeronomy, 2016, Vol. 56, No. 4, pp. 448–456.
[18] D.V. Blagoveshchensky et al., Impact of the magnetic superstorm on March 17–19, 2015 on subpolar HF radio paths: Experiment and modeling, Advances in Space Research 58 (2016) 835–846.
[19] V.P. Uryadov et al., Impact of heliogeophysical disturbances on ionospheric hf channels. Advances in Space Research, 2017. http://doi.org/10.1016/j.asr.2017.07.003
[20] Elias, A.G., Earth's magnetic field effect on MUF calculation and consequences for hmF2 trend estimates, Journal of Atmospheric and Solar–Terrestrial Physics (2017), http://doi.org/10.1016/j.jastp.2017.03.004.
[21] Hongmei Bai, Modeling M (3000)F2 based on extreme learning machine, Advances in Space Research, Volume 65, Issue 1, January 2020, Pages 107-114. https://doi.org/10.1016/j.asr.2019.09.021
[22] Juh-Woei Lin, Geomagnetic Storm Related to Disturbance Storm Time Indices, European Journal of Environment and Earth Sciences, volume 2, Issue 6, 2021, http://dx.doi.org/10.24018/ejgeo.2021.2.6.199
[23] Olga Maltseva, and Tatyana Nikitenko, The effect of space weather on the ionosphere at the 110° meridian during CAWSES-II period, Geodesy and Geodynamics, 2021, Volume 12, Issue 2, Pages 93-101. https://doi.org/10.1016/j.geog.2021.03.001.
[24] Ali Hussein Ni'ma. The Calculation and Analysis of the Total Electron Content Over Different Latitudes and Seasons Using the Numerical Trapezoidal and Simpson Methods. Baghdad Science Journal Vol. 16 (4) Supplement 2019. http://dx.doi.org/10.21123/bsj.2019.16.4(Suppl.).1043
[25] Ayomide O. Olabode and Emmanuel A. Ariyibi, Geomagnetic storm main phase effect on the equatorial ionosphere over Ile–Ife as measured from GPS observations, Scientific African, volume (9) (2020) e00472. https://doi.org/10.1016/j.sciaf.2020.e00472
[26] Juan A. Lazzús et al., Intense Geomagnetic Storms in The Maximum Phase of Solar Cycle 24 Observed From a Low-Latitude Ground Station. Geofísica Internacional (2022) 61-4: 267-286. https://doi.org/10.22201/igeof.00167169p.2022.61.4.2028.
[27] Bodo W. Reinisch and Ivan A. Galkin, Global Ionospheric Radio Observatory (GIRO), Earth Planets Space volume (63), 377–381, 2011. https://doi:10.5047/eps.2011.03.001.
[28] Miteva, R.; Samwel, S.W., Catalog of Geomagnetic Storms with Dst Index ≤ 50 nT and Their Solar and Interplanetary Origin (1996–2019), Atmosphere 2023, 14, 1744. https://doi.org/10.3390/atmos14121744
[29] J. Matzka, The Geomagnetic *Kp* Index and Derived Indices of Geomagnetic Activity Space Weather, 19, e2020SW002641. 2021. https://doi.org/10.1029/2020SW002641
[30] Maurits Kaptein, Edwin van den Heuvel. Statistics for Data Scientists: An Introduction to Probability, Statistics, and Data Analysis, 2020. Springer. ISBN: 303010530X; 9783030105303.